Effect of Through-Thickness Macro and Micro-Texture Gradients on Ridging of 17%Cr Ferritic Stainless Steel Sheet

Moo-Young Huh[1)], Jae-Hyup Lee[1)], Soo Ho Park[2)], Olaf Engler[3)], Dierk Raabe[4)]

[1)]Division of Materials Science and Engineering, Korea University, Seoul, Korea; [2)]Stainless Steel Research Group, Technical Research Laboratories, POSCO, Pohang, Korea; [3)]Hydro Aluminium Deutschland GmbH, R+D Center Bonn, Bonn, Germany; [4)]Max-Planck-Institut für Eisenforschung GmbH, Düsseldorf, Germany

In order to study the formation of ridging in ferritic stainless steel (FSS) sheets, the evolution of the crystallographic texture was investigated by macro and micro-texture measurements throughout the thickness of the sheets. The as-received hot band material displayed a pronounced through-thickness texture gradient with a strong rotated cube orientation in the sheet center layer. The initial texture of the hot band had a high impact on the formation of the cold rolling texture and on the final recrystallization texture. Modification of the cold rolling texture by means of cross-rolling led to an improvement of the macro and micro-textures after final recrystallization annealing, which gave rise to an enhanced sheet formability in FSS. Tensile tests of specimens with half thickness revealed that ridging formed in the sheet center was much stronger than that in the surface. This observation was attributed to the more frequent formation of orientation colonies in the sheet center when compared to the sheet surface.

Keywords: ferritic stainless steel, ridging, macro-texture, micro-texture, recrystallization

Introduction

The formation of preferred crystallographic orientation distributions during the thermomechanical processing of steels may give rise to anisotropic materials properties [1]. A proper control of the crystallographic texture is essential in order to improve the formability of steel sheets [1-4]. In low carbon steel, cold rolling and subsequent recrystallization annealing typically leads to the formation of γ-fiber textures. The (complete) γ-fiber refers to a texture which comprises all orientations with a common crystallographic {111} plane parallel to the sheet surface. Such an orientation distribution provides the desired high planar anisotropy and good deep drawability of low carbon steel sheets [4-14]. The *R*-value (Lankford parameter) is a measure of the planar anisotropy of sheet material. As an example, the *R*-value of cold rolled and recrystallization annealed low carbon steel sheets often exceeds a value of 2.0.

Ferritic stainless steels (FSS), however, often reveal, instead of such a perfectly aligned pronounced γ-fiber texture, a deviation from the exact <111> fiber axis after recrystallization, namely, a texture maximum at {334}<483> [14-17]. The formability of FSS is generally inferior to that of low carbon steels because these steels display a lower *R*-value which is attributed to the overall texture of this material, i.e. to the *macro-texture* [14-20]. Furthermore, undesir-

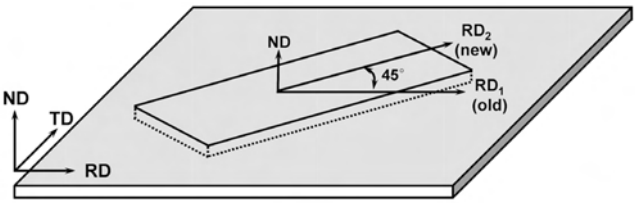

Figure 1. Schematic diagram of the cross-rolling procedure as employed in the present study.

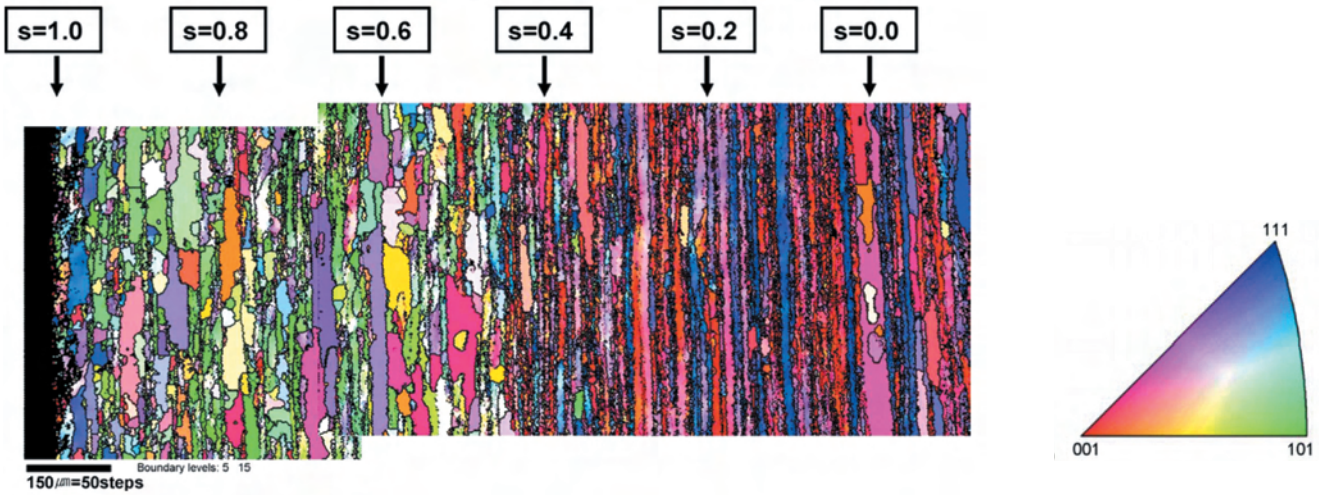

Figure 2. (a) Texture mapping using an inverse pole figure (IPF) coding indicating the crystal axis of each point relative to the sheet normal direction ND.

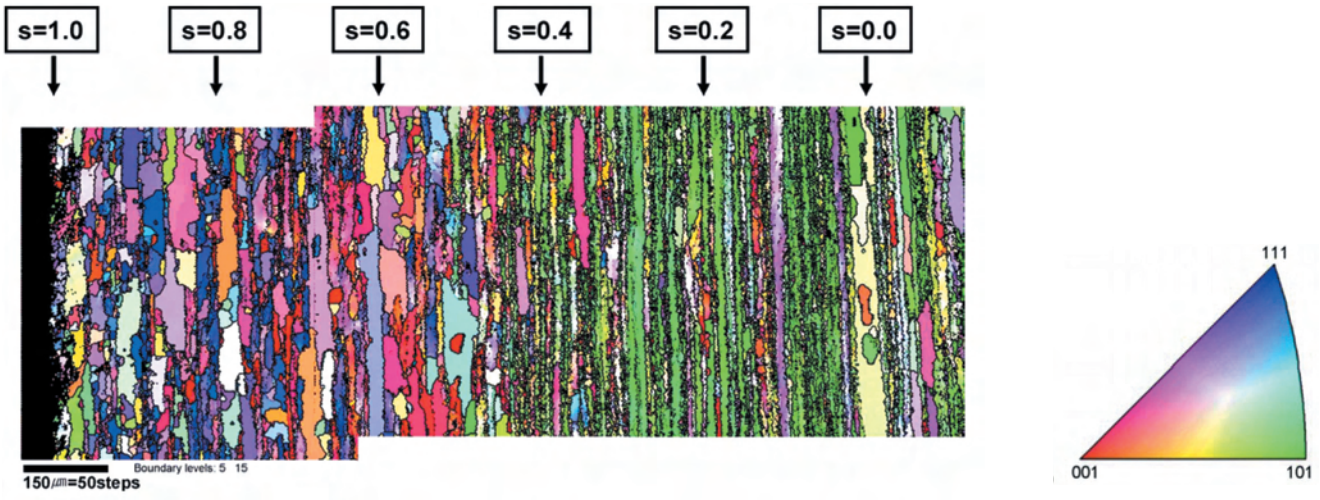

Figure 2. (b) Texture mapping using an inverse pole figure (IPF) coding indicating the crystal axis of each point relative to the sheet rolling direction RD of the hot band material. The observed direction is the transverse direction TD.

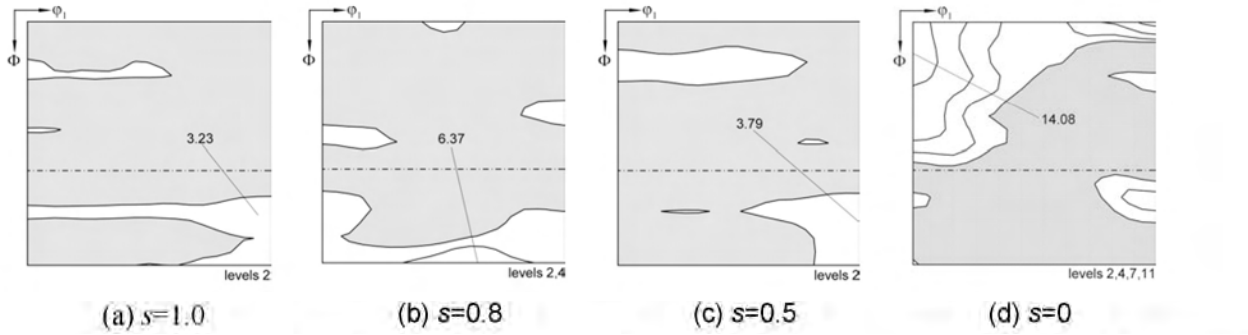

Figure 3. Texture of the hot band at various through-thickness layers. (a) *s*=1.0, (b) *s*=0.8, (c) *s*=0.5, (d) *s*=0.

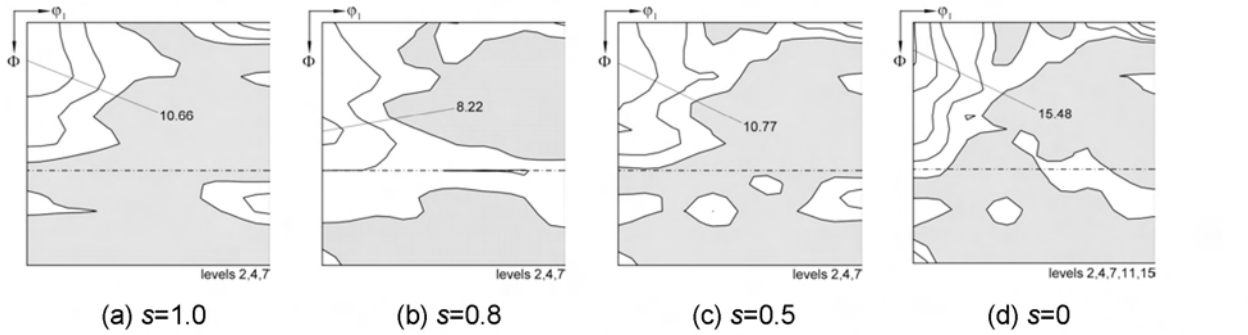

Figure 4. Textures of the conventionally rolled sheet after 80% thickness reduction. (a) *s*=1.0, (b) *s*=0.8, (c) *s*=0.5, (d) *s*=0.

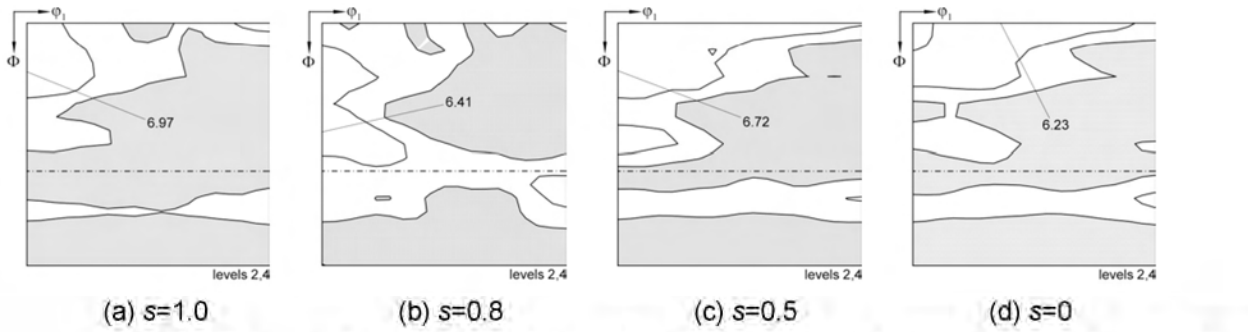

Figure 5. Textures of the cross-rolled sheet after 80% thickness reduction. (a) *s*=1.0, (b) *s*=0.8, (c) *s*=0.5, (d) *s*=0.

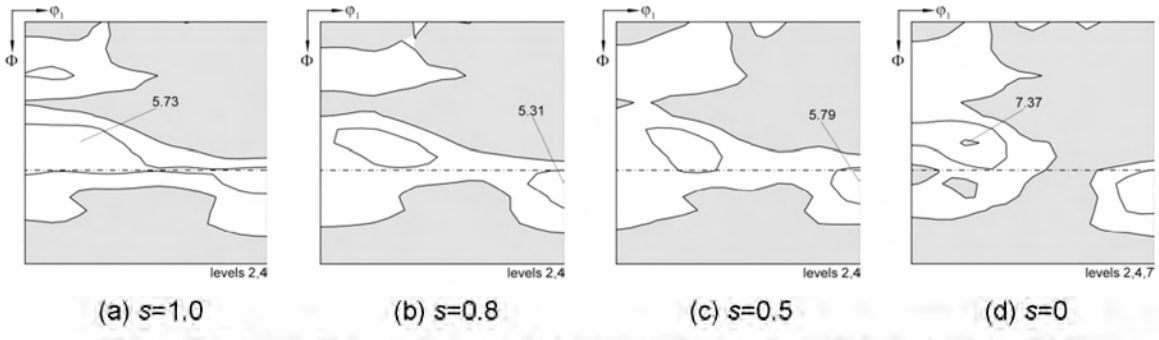

Figure 6. Recrystallization textures of the conventionally rolled sheet after 80% thickness reduction. (a) *s*=1.0, (b) *s*=0.8, (c) *s*=0.5, (d) *s*=0.

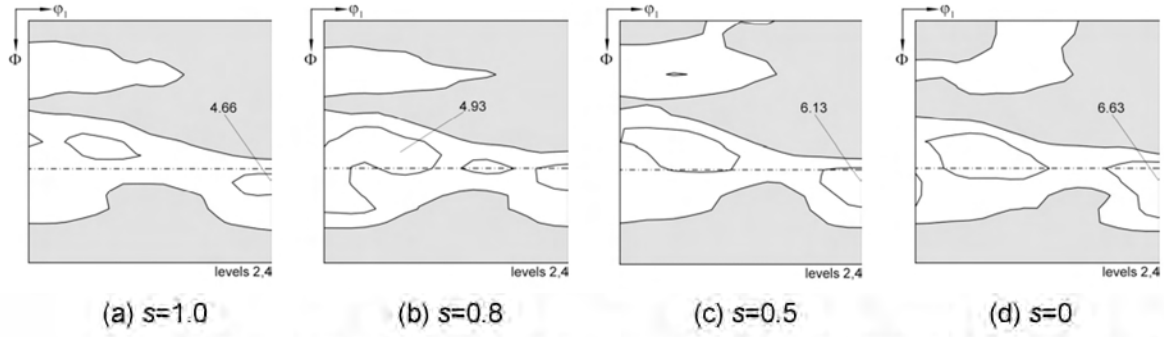

Figure 7. Recrystallization textures of the cross-rolled sheet after 80% thickness reduction. (a) *s*=1.0, (b) *s*=0.8, (c) *s*=0.5, (d) *s*=0.

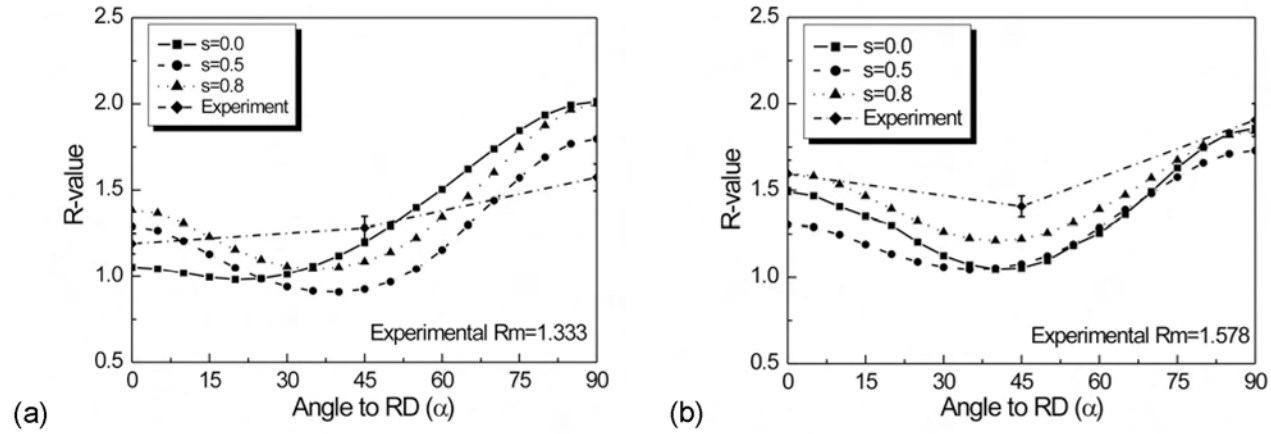

Figure 8. Comparison of experimental and predicted *R*-values (Lankford values) for the two differently processed sheets. (a) conventionally rolled sample, (b) cross-rolled sample.

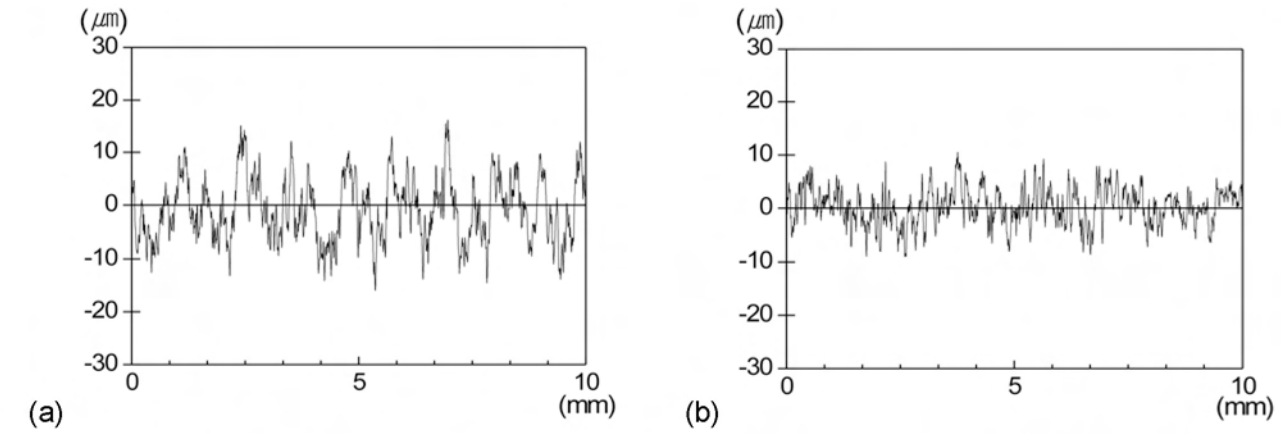

Figure 9. Roughness profiles assessed from the tensile test specimen strained 10% parallel to RD. Measured from (a) the surface (*s*=1.0) of the conventionally rolled sample, (b) the surface (*s*=1.0) of the cross-rolled sample.

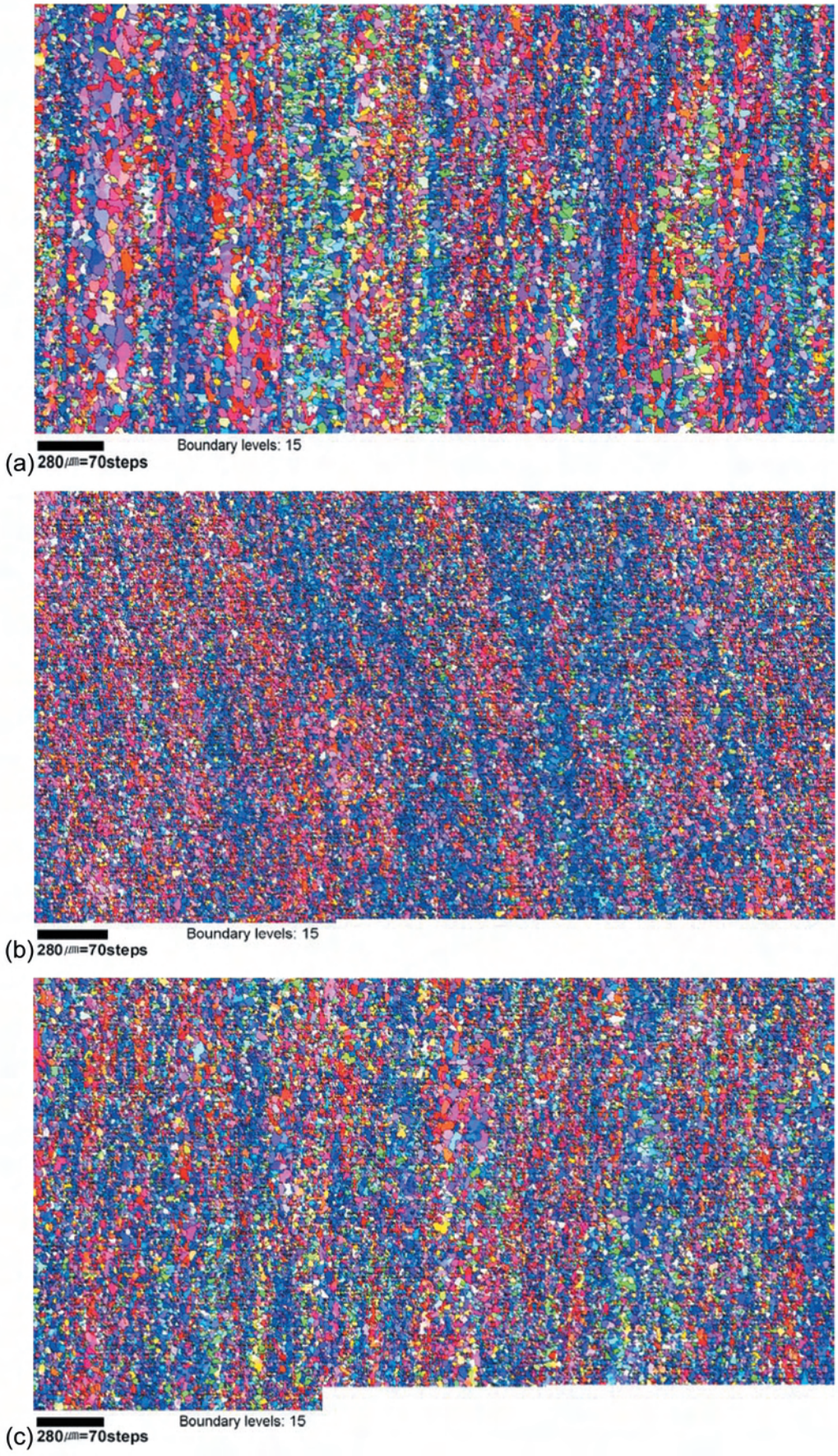

Figure 10. EBSD mapping (using a colour code for the crystallographic axis parallel to ND) of recrystallized FSS sheets; measured from (a) the center layer (s=0) of the conventionally rolled sample, (b) the center layer (s=0) of the cross-rolled sample, (c) the layer close to surface (s=0.8) of the conventionally rolled sample.

able surface defects of ridges or respectively ropes with a depth of 20–50 μm appear during deep drawing [21]. The formation of these surface defects is in the literature mainly attributed to the inhomogeneous distribution of orientations of individual grains, i.e. to the *micro-texture*.

Models of Chao [22], Takechi et al. [23] and Wright [24] have proposed the orientation dependent anisotropy of the plastic deformation which results in ridging. Each of these models provides a potentially plausible physical picture of the ridging phenomenon. In an electron backscattered diffraction (EBSD) study conducted by Brochu et al. [25] the authors suggest that the anisotropic mechanical response of grain colonies or respective grain clusters in FSS upon loading may cause ridging. Recently, ridging in FSS was successfully modeled by the crystal plasticity finite element method (CPFEM) [26]. However, detailed studies on both macro- and micro-texture profiles conducted throughout the thickness of FSS and their effects on ridging are still very limited.

Therefore, in the present work, the evolution of textures in FSS is investigated in four different thickness layers by way of macro- and micro-texture measurements. In order to vary the amount and the magnitude of the surface undulations caused by the ridging phenomenon in FSS, the cold rolling texture and the recrystallization texture were modified by means of cross-rolling [27,28]. The formability of the final sheet material was assessed by standard *R*-value measurements. Riding was studied through the measurement of the surface roughness.

Experimental Procedure

In this study a hot rolled coil with a thickness of 3.05 mm of a commercial ferritic stainless steel (FSS) grade with a chromium content of about 17wt.% was supplied by POSCO, Korea. The exact chemical composition of the ferritic stainless steel is given in **table 1**. A part of this hot band was conventionally cold rolled to a total engineering thickness reduction of 80%, corresponding to a logarithmic strain of ε=1.6. In order to modify the cold rolling texture and to modify the final recrystallization texture, another set of hot band specimens was subjected to cross-rolling. In this study cross-rolling refers to a procedure in which the rolling direction (RD) is rotated once by 45° about the sheet normal direction (ND) before the ensuing standard cold rolling, **figure 1**. The cross-rolled sample was also cold rolled to a total thickness reduction of 80% by maintaining the new rolling direction. For the final recrystallization annealing treatment, both the conventionally cold rolled and the single-step cross-rolled sheets were annealed for 1 h at 750°C in a salt bath furnace.

The *macro-textures* were determined by means of conventional X-ray texture analysis [29,30]. From three incomplete experimental pole figures, the orientation distribution functions (ODF) $f(g)$ were calculated by using the series expansion method according to Bunge (the maximum series expansion degree, l_{max}, amounted to 22) [30]. The orientations g are expressed in form of Euler angles in Bunge notation (φ_1, Φ, φ_2). In order to investigate the texture variation through the sheet thickness, texture measurements were carried out at four different through-thickness layers of the rolled sheets. The inspected layer is described by the parameter $s=a/(d/2)$ with a being the distance of the actual layer from the center layer and d the sample thickness, i.e. s=0 corresponds to the center layer and s=1 to the surface layer. The layers inspected in this study are s=0.0, 0.5, 0.8 and 1.0, i.e. the center layer (s=0.0), the mid-thickness layer between center and surface (s=0.5), a layer close to the surface (s=0.8) and the immediate sheet surface (s=1.0), respectively. The center and the near-surface layers are particularly relevant for texture analysis since they typically show the strongest plane-strain textures (s=0) and shear textures (s=0.8) after rolling, respectively [9,15,31].

For *micro-texture* characterization, electron backscatter diffraction (EBSD) measurements were carried out in a scanning electron microscopy (SEM) equipped with a Schottky field emission (SFE) electron gun. Data acquisition was conducted in the rolling planes (viewed from ND) and longitudinal sections (viewed from TD) of various thickness layers.

Tensile tests were employed in order to determine the *R*-values for each specimen. Samples with dimensions 20mm x 100mm were strained by 10% at a constant crosshead velocity of 10^{-3}/s. For the *R*-value measurements tensile tests were performed with the tensile axis oriented at angles, α, of 0°, 45° and 90° to the sheet rolling direction, RD, respectively. The *R*-value for a given tensile direction is then determined as the ratio between the in-plane and the through-thickness strains.

The occurrence of ridging was assessed through roughness measurements on the surfaces of tensile test specimens which were prepared from the cold rolled and subsequently recrystallized sheets. In order to reveal the effect of the thickness layers on ridging, tensile specimens with half sheet thickness were examined. For that purpose, a tensile test specimen was prepared from the normally rolled and recrystallized sheet by removing half of the thickness of the sheet by grinding and polishing. Thus, the two surfaces of this sample correspond to center (s=0) and surface (s=1) of the original material, respectively.

Experimental Results

The EBSD montage in **figure 2** shows the microstructure of the initial hot band observed from the transverse direction (TD). These figures are so-called inverse pole figure

Table 1. Composition of the ferritic stainless steel according to the chemical analysis (mass content in %)

C	Si	Mn	Cr	Ni	P	Co	Mo	Cu	V	Nb	W	S	Al
0.05	0.34	0.37	16.9	0.19	0.02	0.036	0.012	0.043	0.1	0.018	0.011	0.002	0.003

(IPF) maps, where each grain is colour-coded according to its crystal direction parallel to the ND (figure 2(a)) and RD (figure 2(b)); the corresponding colour code is given. Obviously, the microstructure is very inhomogeneous through the sheet thickness. Highly RD elongated grains can be observed in thickness layers between the sheet center (s=0.0) and the mid-thickness layer (s=0.5). In these layers, very coarse pancake-shaped grains with longitudinal extensions of some hundred μm can be observed. As is evident from the colour code of the inverse pole figures indicating RD and ND directions most of the pancake-shaped grains have orientations close to the rotate cube component {001}<110> [32,33]. The thickness layers from the surface (s=1.0) to the mid-thickness layer (s=0.5) display partly recrystallized grains with a rather irregular shape.

Since most of the relevant orientations and fibers of steel textures appear in the φ_2=45° section of the ODF [7,9,13], the analysis of this section yields a very condensed representation of the most important texture features required for the discussion of the data.

Figure 3 shows the *macro-texture* of the as-received hot band material at the various through-thickness layers investigated. The center layer (s=0.0) shows the typical hot band texture of FSS which is characterized by a pronounced texture consisting of the {hkl}<110> α-fiber with a maximum close to {001}<110> [9,15,34]. This type of texture was found from the center layer (s=0.0) to layers just below the mid-thickness (s=0.5) between center and surface. The mid-thickness layer (s=0.5) and the surface (s=1.0) display more random orientation distributions. A weak orientation scattering along the {011}//ND fiber with a maximum at {011}<211> was observed at the layer s=0.8. When comparing the macro-texture in figure 3 with the micro-texture in figure 2, it can be summarized that the microstructure and texture of the FSS hot band is divided into the center layers having highly elongated grains with orientations close to {001}<110> and the outer layers having less elongated grains in irregular shape with random orientations [9,15,34].

The textures of the 80% conventionally cold rolled specimens are shown in **figure 4** for the various layers s. In the thickness layers s=0.0, 0.5 and 1.0, the rolling textures are dominated by the α-fiber with a maximum at (φ_1,Φ,φ_2)=~(0°,15°,45°) together with a rather weak γ-fiber. In the sheet center (s=0) the strong hot band texture remained very stable during cold rolling and also the position of the maximum $f(g)$-value was hardly shifted. In contrast to other layers, the layer s=0.8 displayed well developed α- and γ-fiber orientations with a maximum at (φ_1,Φ,φ_2)=(0°,45°,45°). This cold rolling texture observed at s=0.8 is quite similar to that commonly observed in low carbon steels (e.g. Ref. [5-10]).

As mentioned in the experimental procedure, the initial texture before cold rolling was varied by cross-rolling in order to modify the cold rolling texture and, thereby, also the final recrystallization texture. In the present work, the initial texture and microstructure of the cross-rolled specimens were rotated 45° about the ND before the further cold rolling. Because the ND-rotation of an orientation (φ_1,Φ,φ_2) by a reorientation angle of 45° corresponds to an orientation change of (φ_1+45°,Φ,φ_2), the main texture component which was formerly at {001}<110> resides after the rotation at {001}<100> in the initial sample prior to further rolling. **Figure 5** shows the textures of the 80% cross-rolled sample. Cold rolling of the cross-rolled specimens gave rise to a weakening of the overall texture, in particular of the <110>//RD α-fiber orientations. The thickness layers s=0.0, 0.5 and 1.0 display orientations on the {001}//ND and {332}//ND fibers. Interestingly, the texture observed in the s=0.8 layer was similar to that of the conventionally rolled sample (figure 4(c)).

After the final recrystallization annealing treatment, the 80% conventionally rolled sheet displayed the typical recrystallization textures of FSS as shown in **figure 6**. The recrystallization texture reveals a maximum at {334}<4$\bar{8}$3> which deviates by about 8° from the exact {111}<112> orientation which is located on the γ-fiber [14,15]. The {334}<4$\bar{8}$3> texture component is more pronounced in the sheet center where an uneven intensity distribution along the γ-fiber is observed.

Figure 7 shows the final recrystallization texture of the 80% cross-rolled sheet. In order to estimate the influence of the cross-rolling procedure on the recrystallization texture, this figure has to be compared with the recrystallization texture of the conventionally rolled sheet (figure 6). This comparison shows that the recrystallization textures of the sheet material which was produced by cross-rolling are somewhat weaker and show a more homogeneous γ-fiber through the sheet thickness. Instead of a texture component at {334}<4$\bar{8}$3>, the maximum orientation density was obtained at {554}<225> at s=0.0, 0.5 and 1.0. Thus, the macro-textures after the final recrystallization were successfully modified by the cross-rolling introduced in the present study.

Discussion

As documented in the literature [14-18, 31], the thermomechanical processes involved in the manufacturing of FSS sheets give rise to pronounced texture and microstructure gradients in the hot band as shown in figures 2 and 3. The texture and microstructure of the FSS hot coil examined in this work can be divided into two distinguished types of through-thickness regimes. The center layers, ranging from the sheet center (s=0.0) to the mid-thickness layer (s=0.5), comprise pancake-shaped grains which are highly elongated in RD with a {hkl}<110> α-fiber texture and a maximum orientation density close to {001}<110> [9,15,32,33]. The outer thickness layers, from the sheet surface (s=1.0) to the mid-thickness layer (s=0.5), consist of partly recrystallized grains with a more equiaxed shape and nearly random textures with weak orientations close to {011}<211> and {011}<100> [9,15,34]. This inhomogeneous texture and microstructure of the initial hot band material strongly affects the further evolution of the texture and microstructure during subsequent cold rolling and recrystallization.

In the present study, the initial texture of the hot band was changed by cross-rolling in order to modify the cold rolling texture and, thereby, also the final recrystallization texture. After the recrystallization treatment, the 80% con-

ventionally rolled sheet displayed the typical recrystallization textures of FSS with a texture maximum at {334}<4$\bar{8}$3> deviating about 8° from the {111}<112> component [9,14,15]. This main texture component is more pronounced in the sheet center layer where also a quite uneven orientation density along the γ-fiber was observed.

Raabe and Lücke have suggested that the evolution of the recrystallization texture component {334}<4$\bar{8}$3> in FSS can be explained in terms of the preferred growth of this component into the {112}<110> deformation component by way of a 'selective particle drag' mechanism [35,36]. Huh and Engler proposed that the orientation {334}<4$\bar{8}$3> might form by way of a growth selection out of the scattered rolling texture in the vicinity of the preexisting grain boundaries, which is facilitated by its high-mobility CSL-grain boundary relative to the {112}<110>-oriented matrix [17]. The present work supports the above arguments on the evolution of {334}<4$\bar{8}$3> in FSS. Comparing the cold rolling textures of the center layer in the conventionally rolled and the cross-rolled samples (figures 4 and 5), the intensity of {112}<110> in the cross-rolled sample is much lower than that of the conventionally rolled sample. After the final recrystallization treatment, the center layer of the conventionally rolled sheet showed a texture maximum at {334}<4$\bar{8}$3>. The center layer of the cross-rolled sheet, in contrast, depicted a quite homogeneous {111}//ND γ-fiber texture.

As mentioned above, the recrystallization textures were successfully modified by the cross-rolling procedure introduced in the present work. In order to evaluate the improvement of the drawability by means of the cross-rolling process, the sheet formability of FSS was investigated by measurements of the *R*-values (Lankford parameters). *R*-values were determined in tensile tests from the ratio between the in-plane and the through-thickness strain for different angles α=0°, 45° and 90°, between tensile direction and rolling direction. For the calculation of a mean value, R_m, the following equation was used

$$R_m = \frac{R_{0^\circ} + 2 \cdot R_{45^\circ} + R_{90^\circ}}{4} \qquad (1)$$

where the subscripts 0°, 45° and 90° denote the angles α between tensile direction and rolling direction. **Figure 8** shows the results for the individual *R*-values of the recrystallized samples. The conventionally rolled sheet yields R_m, values close to 1.33. For the sheet processed via cross-rolling, the average value was notably higher, namely R_m=1.57. Since the planar anisotropy of a sheet mainly depends on the orientation distribution of the grains, i.e. on the *macro*-texture, the corresponding *R*-values can also be directly calculated through the texture [30, 37]. Figure 8 shows the calculated *R*-values for the various through-thickness layers of the two differently cold rolled samples. Data from the surface layer (*s*=1.0) were excluded because of the limited volume contribution of the immediate surface layers. Apparently, the texture gradients through the thickness layers lead to strong variations of the calculated *R*-values as a function of the analysed layer. In the conventionally cold rolled samples (figure 8(a)), the experimental R_{0°-value was smaller than that along R_{45° and R_{90°, which is attributed to the $R(\alpha)$-values calculated with the center layer texture. In figure 8(b), the calculated $R(\alpha)$-values from all thickness layers have their minimum *R*-values in 45° to the RD leading to a small experimental value for R_{45° in the cross rolled sample.

With regard to the development of ridging, the surfaces of the tensile test specimens were examined via roughness measurements. **Figure 9** shows the surface profiles of the two sheets produced by normal rolling and by cross-rolling, respectively. Obviously, the surface of the conventionally rolled sheet was much rougher than that of the cross-rolled sheet. For quantifying the roughness data, the average roughness value, described by R_a, and the maximum roughness value, described by R_t, were determined. The resulting values of R_a=4.3 μm and R_t=24.3 μm for the conventionally rolled sample are almost twice as large as those for the cross-rolled sample (R_a=2.3 μm and R_t=12.7 μm). This result shows that the modification of the cold rolling texture by means of cross-rolling entails the formation of an annealing texture and microstructure which is less prone to undergo severe ridging.

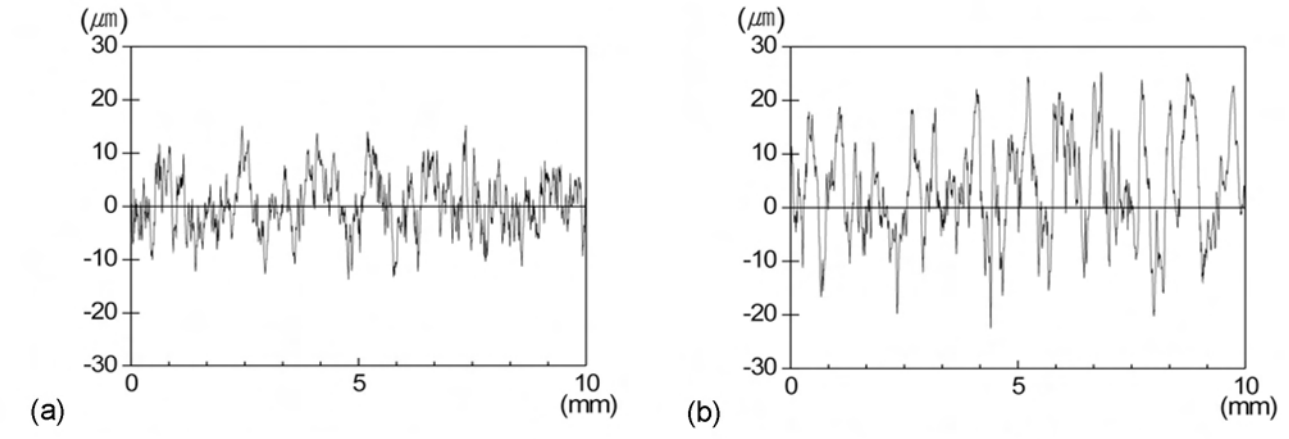

Figure 11. Roughness profiles assessed from the tensile test specimen at half thickness; measured from (a) the surface (*s*=1.0), (b) the center layer (*s*=0).

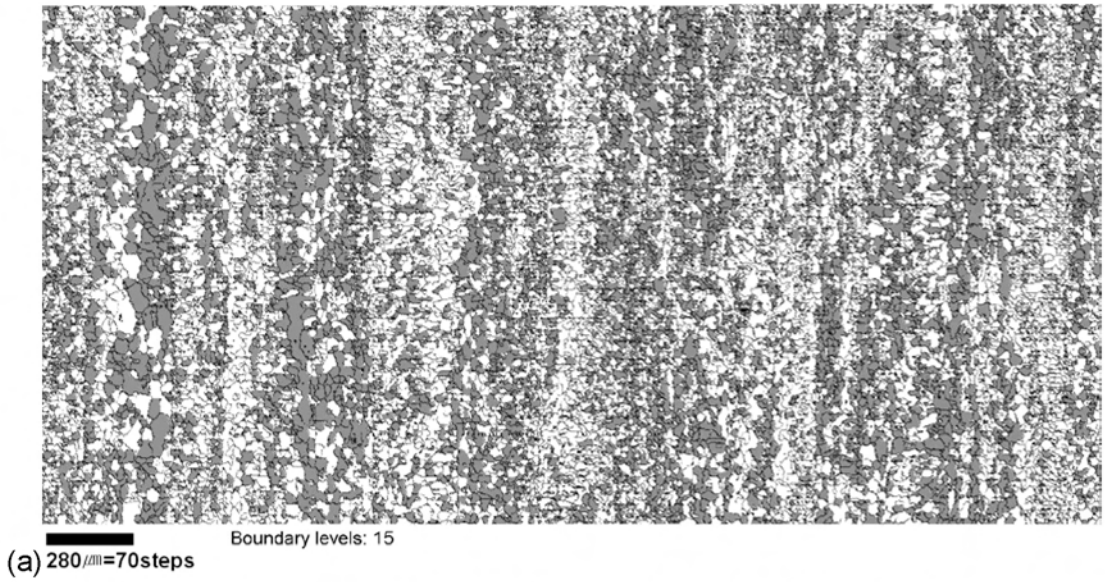

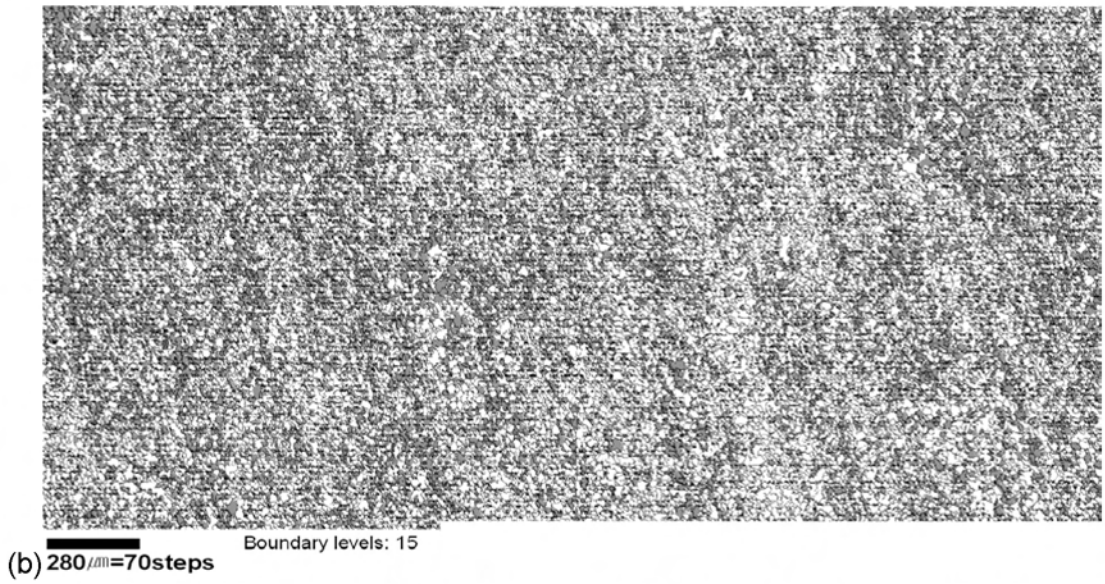

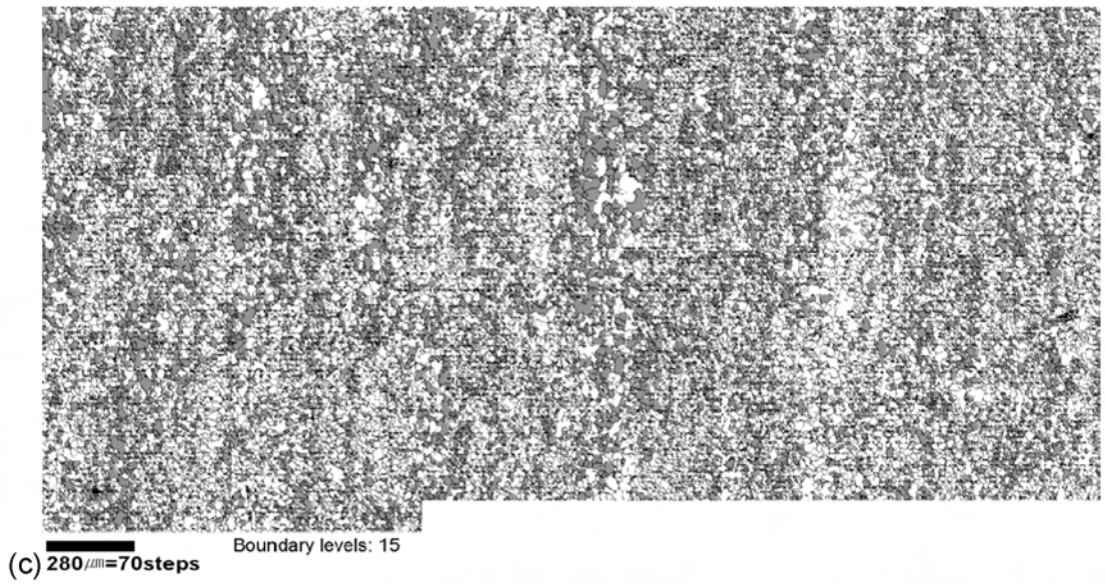

Figure 12. EBSD mapping of the local *R*-values. The gray grains indicate $R < 1$ and the white grains denote $R > 1$. (a) the center layer (s=0) of the conventionally rolled sample, (b) the center layer (s=0) of the cross-rolled sample, (c) the layer close to the surface (s=0.8) of the conventionally rolled sample.

In order to investigate the evolution of the *micro*-texture in an area which is sufficiently large to assess ridging, EBSD measurements were carried out on an area of 3.5mm× 1.7mm. **Figure 10** shows the resulting texture maps in terms of an inverse pole figure (IPF) coding indicating the crystal axis of each point relative to the sheet normal direction. In the conventionally cold rolled and subsequently recrystallized sample the center layer (s=0) observed from the normal direction is characterized by long orientation clusters comprising grains with similar orientations as evident from figure 10(a). Most of the grains which are found in such orientation colonies belong either to the {111}//ND texture fiber (grains in blue colour) or to the {001}//ND texture fiber (grains in red colour). The lateral extension of the orientation clusters is nearly parallel to the rolling direction. Interestingly, the cross-rolled sample displayed its orientation colonies inclined at about ~20º to the rolling direction. The formation of the orientation colonies was less dominant in the cross-rolled sample than in the conventionally rolled specimen, figure 10(b). It is worth mentioning in that context that the initial hot band already contained large pancake-shaped grains in the mid-thickness region between the center and the mid thickness layers, figure 2. It is likely that these large hot band grains are in part inherited through cold rolling and (insufficient) recrystallization to the final material [9,14,15]. Accordingly, we attribute the observed orientation colonies which are frequently observed in FSS to the large grains of the initial hot band material. It was already mentioned that the thickness layers close to the surface reveal a much smaller frequency of such elongated orientation clusters, figure 10(c). This corresponds to the observation that the thickness layers close to the surface of the initial hot band typically contain smaller and more equiaxed grains (figure 2).

Since the phenomenon of ridging in FSS is linked to the formation of orientation colonies [21,25,26], more severe ridging is expected to stem mainly from the material close to the center layers rather than from the sheet surface. In order to elucidate this particular topological effect of the contribution of the texture of the different through-thickness layers to the overall ridging profile, tensile specimens ground to half thickness were prepared and investigated with respect to ridging for the conventionally cold rolled and subsequently recrystallized sheet material. As shown in **figure 11**, the ridging profile originating from the center thickness layer was much rougher than that obtained from samples with additional contributions from the surface layer. Accordingly, it is concluded that the microstructure and the texture particularly of the center thickness layer should be properly controlled in order to diminish ridging in FSS.

The present findings substantiate the assumption that steel sheets containing pronounced orientation colonies tend to form ridging, while sheets with a random micro-texture, i.e. a homogeneous distribution of the grain orientations, are generally free from ridging. This strong impact of grain colonies on ridging is attributed to local variations in the strain response during tensile testing of the final recrystallized FSS sheets. In what follows we will present a simple model which is based on the local variations in *R*-values. Grains in a given orientation colony will possess different *R*-values than grains in the neighbouring orientation colonies. Upon tensile testing, the various grain colonies will deform differently, according to their local R-value. Thus, an inhomogeneous distribution of orientations will lead to macroscopic surface defects, specifically, to ridging. A more detailed study, which includes the effects of both grain colonies with varying R-values and alternating arrangements of orientation clusters with opposite out-of-plane shears, will be presented in a separate paper [37].

Calculation of the *R*-values using the minimum deformation work principle [30,38] shows that among the typical b.c.c. recrystallization texture components the orientation {001}<110> has the minimum *R*-value, and the α fiber orientations in a range within 40° from {001}<110> all have low *R*-values smaller than 1. Vice versa, maximum *R*-values are obtained for the γ–fiber orientations with {111}//ND. **Figure 12** shows EBSD maps where orientations (i.e., measured points) with *R*-values below 1 are shaded in grey. The white grains in figure 12 indicate their *R*-values higher than 1. It turns out that in the center layer (*s*=0) of the conventionally rolled and recrystallized sample with strong ridging, grey grains and white grains are clustered together and form bands aligned parallel to the RD. In contrast, in the center layer of the cross-rolled sample with strongly reduced ridging the grey and white grains are distributed more or less uniformly. The formation of clustered bands comprising white or grey grains was less pronounced in the layers close to the surface (s=0.8) of both conventionally rolled and cross-rolled samples.

Conclusions

The macro and micro-textures of the initial hot band material have a strong influence on the further evolution of textures in cold rolled and recrystallized ferritic stainless steel sheet. Modification of the initial texture and microstructure by means of 45° ND cross-rolling led to an improvement of the macro and micro-textures in the finally recrystallized sheets. These modifications entailed an enhanced planar anisotropy and less severe ridging. The correlation of the local riding profiles taken from tensile specimens with half thickness and corresponding EBSD orientation maps showed that elongated orientation colonies formed close to the sheet center are responsible for ridging in cold rolled and recrystallized ferritic stainless steel sheet.

Acknowledgments

The authors gratefully acknowledge the financial support of POSCO.

(A2005053; received on 22 December 2004)

Contact:
Prof. Dr.-Ing. Moo-Young Huh
Division of Materials Science and Engineering,
Korea University
Seoul 136-701, Korea
E-mail address: myhuh@korea.ac.k

References

[1] H.J. Bunge and W.T. Roberts: J. Appl. Cryst., 2 (1969), 116.
[2] W.B. Hutchinson: Intern. Met. Rev., 29 (1984), 25.
[3] R.K. Ray, J.J. Jonas and R.E. Hook: Intern. Mater. Rev., 39 (1994), 129.
[4] D. Raabe, P. Klose, B. Engl, K.-P. Imlau, F. Friedel, F. Roters: Advanced Engineering Materials, 4 (2002), 169.
[5] M. Y. Huh, H. C. Kim, and O. Engler: Steel Research, 71 (2002), 239.
[6] M.Y. Huh, Y.S. Cho, J.S. Kim and O. Engler: Z. Metallkunde, 90 (1999), 124.
[7] U. v. Schlippenbach, F. Emren and K. Lücke: Acta Metall., 34 (1986), 1289.
[8] L.S. Tóth, J. J. Jonas, D. Daniel and R.K. Ray: Metall. Trans., 21A (1990), 2985.
[9] M. Hölscher, D. Raabe and K. Lücke: Steel Research, 62 (1991), 567.
[10] M.Y. Huh, D. Raabe and O. Engler: Steel Research, 66 (1995), 353.
[11] E. J. Shin, B. S. Seong, C. H. Lee, H. J. Kang and M. Y. Huh: Steel Research Int., 74, (2003), 356.
[12] E. Shin, B. S. Seong, H. J. Kang and M. Y. Huh: Z. Metallkunde, 94 (2003), 1234.
[13] F. Emren, U. v. Schlippenbach and K. Lücke: Acta Metall., 34 (1986), 2105.
[14] D. Raabe and K. Lücke: Scripta Metall., 27 (1992), 1533.
[15] D. Raabe and K. Lücke: Mater. Sci. Technol., 9 (1993), 302.
[16] D. Raabe, M. Hölscher, M. Dubke, H. Pfeifer, H. Hanke, K. Lücke: Steel Research, 64 (1993) 359.
[17] M. Y. Huh and O. Engler: Mater. Sci. Eng., A308 (2001), 74.
[18] D. Raabe: J. Mater. Sci., 31 (1996), 3839.
[19] T. Sakai, Y. Saito, M. Matsuo and K. Kawasaki: ISIJ Int., 31 (1991), 86.
[20] R. Paton: Mater. Sci. Technol., 10 (1994), 604.
[21] S. H. Park, W. Y. Kim, Y. D. Lee and C. G. Park: ISIJ Int., 42 (2002), 100.
[22] H.C. Chao: Trans. ASM, 60 (1967), 37.
[23] H. Takechi, H. Kato, T. Sunami and T. Nakayama: Trans. JIM, 31 (1967), 717.
[24] R.N. Wright: Metall. Trans., 3 (1972), 83.
[25] M. Brochu, T. Yokota and S. Satoh: ISIJ Int., 37 (1997), 872.
[26] H. J. Shin, J. K. An, S. H. Park and D. N. Lee: Acta Mater., 51 (2003), 4693.
[27] M.Y. Huh, O. Engler and D. Raabe: Textures and Microst., 24, (1995), 225.
[28] M. Y. Huh, S. Y. Cho and O. Engler: Mater. Sci. Eng., A315/1-2, (2001), 35.
[29] V. Randle, O. Engler: Introduction to Texture Analysis: Macrotexture, Microtexture and Orientation Mapping, Gordon and Breach Science Publ., Amsterdam, 2000.
[30] H.J. Bunge: Texture Analysis in Materials Science, Butterworths, London, 1982.
[31] D. Raabe: Steel Research Int., 74 (2003), 327.
[32] D. Raabe: Steel Research, 66 (1995), 222.
[33] D. Raabe, Z. Zhao, S.–J. Park, F. Roters: Acta Materialia 50 (2002) 421
[34] D. Raabe, M. Ylitalo: Metallurgical and Materials Transactions A, 27 (1996) 49.
[35] D. Raabe: Mater. Sci. Technol., 11 (1995), 461.
[36] D. Raabe and K. Lücke: Scripta Metall., 27 (1992), 19.
[37] O. Engler, M. Y. Huh, C. N. Tomé: accepted for publication in Metallurgical and Materials Transaction A, 36 (2005).
[38] H. J.Bunge: Kristall u.Technik, 5 (1970), 145.